Títol del treball:

Towards an accurate Kohn-Sham Density Functional Theory Molecular Energy Decomposition scheme.

Estudiant: Martí Gimferrer Andrés Grau en Química
Correu electrònic: mgimferrer18@gmail.com

Tutor: Pedro Salvador Sedano
Cotutor*:
Empresa / institució: Universitat de Girona

Vistiplau tutor (i cotutor*):

Nom del tutor: Pedro Salvador Sedano
Nom del cotutor*:
Empresa / institució: Universitat de Girona
Correu(s) electrònic(s): pedro.salvador@udg.edu

*si hi ha un cotutor assignat

Data de dipòsit de la memòria a secretaria de coordinació: 30/05/2016

SUMMARY

The most important result of a quantum chemical calculation is the total energy of the molecular system. However, being a single number, it provides little immediate chemical information. Energy decomposition schemes provide additional chemical information by decomposing the total energy of a molecular system into the sum of atomic and diatomic contributions.

In this work we have implemented in the program APOST3D the Kohn-Sham Density Functional Theory (KS-DFT) energy partitioning for open-shell system for a number of pure and hybrid DFT functionals. This has permitted to study in some detail some polyradical systems, but most importantly it will allow us in the future to apply the methodology to transition metal complexes.

The KS-DFT energy decomposition differs from the well-established Hartree-Fock (HF) one on the exchange-correlation term. Within DFT these contributions are obtained solely from one-electron integrations, whereas in HF they originate from two-electron ones. The extremely good correlations we have obtained for a set of molecules between both schemes provides the opportunity to calculate hybrid KS-DFT exchange energies or even the exact HF ones from pure KS-DFT exchange expressions, thus dramatically reducing the computational cost.

Finally, one of the technical problems of these energy decomposition schemes is the evaluation of the necessary 6D numerical integrations, basically because of their large integration error associated. In this work, an improvement of the numerical integration method for the two-electron one-center numerical integration has been developed, based on the double rotation of a second set of integration grid points. The new scheme has been implemented first using a simple model, and then into the APOST3D program. The results obtained are promising, but further studies using a more diverse set of molecules including transition metal complexes are required.

RESUMEN

El resultado más importante procedente de un cálculo de estructura electrónica es la energía total del sistema molecular. Ésta, debido a ser un solo número, nos proporciona escasa información química. Los métodos de descomposición de la energía nos apostaran información adicional, descomponiendo la energía total del sistema como la suma de contribuciones atómicas y diatómicas.

En este trabajo, hemos implementado para sistemas de capa abierta la partición de la energía Kohn-Sham, dentro el marco de la teoría del funcional de la densidad, al programa APOST3D para una serie de funcionales de la densidad puros i híbridos. Este hecho nos ha permitido estudiar en detalle sistemas poliradicales y nos abre las puertas a aplicar esta metodología para complejos que contengan metales de transición en un futuro.

Los métodos de descomposición de la energía KS-DFT difieren del método exacto HF (HF) en el término de la energía de intercambio y correlación. En el marco DFT, estas contribuciones se obtienen únicamente mediante integrales monoelectrónicas, mientras que en el caso HF se requieren integrales bielectrónicas. Las extremadamente buenas correlaciones obtenidas entre los dos métodos nos proporcionan la oportunidad de calcular la energía de intercambio para funcionales KS-DFT híbridos y hasta HF mediante las expresiones de la energía de intercambio para funcionales KS-DFT puros, disminuyendo potencialmente el coste computacional.

Finalmente, uno de los problemas técnicos de los métodos de la descomposición de la energía proviene de la necesidad de realizar integrales numéricas 6D, debido a su alto error de integración asociado. En este trabajo, se ha desarrollado una mejora del método de integración numérica para integrales de un centro y dos electrones, basada en la doble rotación del segundo conjunto de puntos de integración. La implementación de este método se ha realizado primero utilizando un sistema modelo y posteriormente al programa APOST3D. Los resultados obtenidos son prometedores, aunque es necesaria la continuación del estudio para un conjunto más diverso que incluya complejos con metales de transición.

RESUM

El resultat més important precedent d'un càlcul d'estructura electrònica és l'energia total del sistema molecular. Aquest, degut a ser un únic nombre, ens proporciona escassa informació química. Els mètodes de descomposició de l'energia aportaran informació addicional, descomponent l'energia total del sistema com a suma de contribucions atòmiques i diatòmiques.

En aquest treball, hem implementat per sistemes de capa oberta la partició de l'energia Kohn-Sham, dins el marc de la teoria del funcional de la densitat, al programa APOST3D per una sèrie de funcionals de la densitat purs i híbrids. Aquest fet ens ha permès estudiar en detall sistemes poliradicals i ens obra les portes a aplicar aquesta metodologia per complexos que continguin metalls de transició en un futur.

Els mètodes de descomposició de l'energia KS-DFT difereixen del mètode exacte Hartree-Fock (HF) en el terme de l'energia d'intercanvi i correlació. Dintre DFT, aquestes contribucions s'obtenen solament a partir d'integrals monoelectròniques, mentre que en HF procedeixen d'integrals bielectròniques. Les extremadament bones correlacions obtingudes entre els dos mètodes ens proporcionen l'oportunitat de calcular l'energia d'intercanvi per funcionals KS-DFT híbrids o fins i tot HF a partir de les expressions de l'energia d'intercanvi per funcionals KS-DFT purs, disminuint potencialment el cost computacional.

Finalment, un dels problemes tècnics dels mètodes de descomposició de l'energia prové de la necessitat de realitzar integrals numèriques 6D, degut al seu alt error d'integració associat. En aquest treball, s'ha desenvolupat una millora del mètode d'integració numèrica per integrals d'un centre i dos electrons, basada en la doble rotació del segon conjunt de punts d'integració. La implementació d'aquest mètode s'ha realitzat primer utilitzant un sistema model i posteriorment al programa APOST3D. Els resultats obtinguts són prometedors, tot i que és necessari la continuació de l'estudi utilitzant un conjunt més divers de molècules incloent complexos amb metalls de transició.

INDEX

SUMMARY II

RESUMEN III

RESUM IV

1. INTRODUCTION 1

1.1. Traditional methods for energy partitioning 1

1.2. Atomic partitioning of the 3D-space 2

1.3. Molecular energy partitioning in 3D-space 3

1.4. KS-DFT energy partitioning 7

2. OBJECTIVES 9

3. METHODOLOGY 10

3.1. Computational details 10

3.2. 3D numerical integrations 10

3.3. A note on sustainability 12

4. RESULTS AND DISCUSSION 13

4.1. Optimization of the rotational angles on a 6D integral 13

4.2. Implementation of unrestricted KS-DFT energy decomposition 18

4.3. Application to polyradical systems 19

4.4. HF vs DFT atomic and diatomic exchange terms. 22

4.5. HF vs DFT total atomic and diatomic contributions 24

5. CONCLUSIONS AND PERSPECTIVES 29

BIBLIOGRAPHY 30

1. INTRODUCTION

1.1. Traditional methods for energy partitioning

The most important result of a quantum chemical calculation is the total energy of the molecular system. However, being a single number, it carries little immediate chemical information to us. One thing that can provide chemical information is trying to decompose the total energy into contributions that are relevant from a chemical point of view, e.g. the interaction between two atoms.

One of the most typical energy decomposition is the so-called Energy Decomposition Analysis[1] (EDA). It is based on dividing the molecule into two interacting fragments that can react forming the molecule. One example could be the one in figure 1.

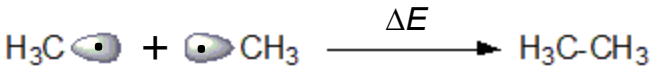

Figure 1. Interaction between two identically described methyl radical forming ethane.

With this partition, we can achieve the overall stabilization energy ΔE of the molecule with respect to the two fragments. Within EDA, this energy can be first decomposed into

$$\Delta E = \Delta E_{prep} + \Delta E_{\text{int}} . \quad (1)$$

The first term is the preparation energy, ΔE_{prep}, which is defined as the amount of energy required for the deformation of the geometry of each fragment in their "equilibrium" to the geometry that they achieve after interacting between them. The second term is the interaction energy, ΔE_{int}, which is defined as the energy change when the two fragments are joined to form the final molecule. This interaction energy can be further decomposed in four different contributions

$$\Delta E_{int} = \Delta E_{elstat} + \Delta E_{Pauli} + \Delta E_{oi} + \Delta E_{disp} , \quad (2)$$

namely, electrostatic interaction, Pauli repulsion, orbital interaction and dispersion.

When applying EDA within density functional theory (DFT), the ΔE_{disp} is added as an additional term accounting for the van der Waals interaction correction to the DFT energy.

A different energy decomposition scheme for the total energy of a molecule was proposed in 2001 by Salvador et al.[2] Unlike the EDA, this molecular energy

decomposition does not require a definition of interacting fragments, and decomposes the total energy of the system into one-center (atomic) and two-center (diatomic) contributions.

$$E = \sum_A E_A + \sum_{A,B<A} E_{AB} \,. \tag{3}$$

The one-center terms account for the effective energy of each atom within the molecule, whereas the two-center terms reflect the attractive/repulsive interactions between every pair of atoms that are responsible of the molecule stability.

The partitioning of the 3D-space on atomic domains is necessary to apply such energy decomposition scheme. That is, one must be able to define the atom within the molecule. There are several approaches to this end.

1.2. Atomic partitioning of the 3D-space

The most important methods that account for the definition of the atom within the molecule by dividing the physical 3D-space are the Quantum Theory of Atoms in Molecules (QTAIM)[3,4] and the fuzzy atoms.[5] In both of them each atom is defined as its nucleus and a region of the space surrounding it.

In the QTAIM framework, the 3D-space is divided into atomic regions using information from the electron density in such a way that each point of the space belongs to a given atom. The set of points conform the atomic domain. On the contrary, fuzzy atoms are allowed to overlap. For each atom A and every point of the 3D-space, a weight function, $w_A(\vec{r})$, is introduced in order to measure to what extent the point contributes to the respective atom. The weight functions must satisfy the following two conditions

$$\sum_A w_A(\vec{r}) = 1 \qquad\qquad w_A(\vec{r}) \geq 0 \,. \tag{4}$$

QTAIM atoms can also be defined using such weight functions, being their values at a point $\vec{r}$ either 0 or 1. In fuzzy atoms they can take any value between 0 and 1.

There are different schemes within the fuzzy atom framework. In this work we have used the so-called Topological Fuzzy Voronoi Cells (TFVC),[6] a scheme that provides results similar to those obtained with QTAIM but at much lower computational cost.

Once a partition of the 3D-space has been established, one can obtain the atomic contributions of a given quantity expressed as a one-electron integral either by

restricting the integration over the atomic domain, or by introducing the appropriate atomic weight function

$$\int_{\Omega_A} f(\vec{r})d\vec{r} \equiv \int w_A(\vec{r})\, f(\vec{r})d\vec{r} = N_A \,. \tag{5}$$

Similarly, a two-electron integral will naturally decompose into both atomic (if both electrons lie on the same atomic domain) and diatomic (if each electron lies in a different atomic domain) contributions.

1.3. Molecular energy partitioning in 3D-space

In 2001 Salvador et al.[2] implemented a molecular energy decomposition method for the Restricted Hartree-Fock (RHF) energy. The one- and two-center terms obtained read as

$$\begin{aligned} E_A &= 2\sum_{i=1}^{N/2} < \phi_i \mid -\frac{1}{2}\nabla^2 - \frac{Z_A}{R_A} \mid \phi_i >_A + \sum_{i,j=1}^{N/2} 2\left[\phi_i\phi_j \mid \phi_i\phi_j\right]_{A,A} - \left[\phi_i\phi_j \mid \phi_j\phi_i\right]_{A,A} \\ E_{AB} &= -2\sum_{i=1}^{N/2}\left(< \phi_i \mid \frac{Z_B}{R_B} \mid \phi_i >_A + < \phi_i \mid \frac{Z_A}{R_A} \mid \phi_i >_B \right) + \\ &+ 2\sum_{i,j=1}^{N/2}\left(2\left[\phi_i\phi_j \mid \phi_i\phi_j\right]_{A,B} - \left[\phi_i\phi_j \mid \phi_j\phi_i\right]_{A,B} \right) + \frac{Z_A Z_B}{R_{AB}} \end{aligned} \quad , \tag{6}$$

where *N*/2 is the number of doubly filled molecular orbitals, $\{\phi_i(\vec{r})\}$, and the [12|12] convention is used for the two-electron integrals. In the one electron integrals, the subscript "A" indicates that the integration is performed over the atomic domain Ω_A,

$$\langle \phi_i \mid \hat{h} \mid \phi_i \rangle = \int_{\Omega_A} \phi_i^*(\vec{r})\hat{h}\phi_i(\vec{r})d\vec{r} \,, \tag{7}$$

where $\hat{h}$ represents either the $-\frac{1}{2}\nabla^2$ or $\frac{Z_A}{R_A}$ operators.

In the case of the two-electron integrals, the subscript "A,B" indicates that the integration for the electrons 1 and 2 are carried out over the atomic domains Ω_A and Ω_B respectively.

$$[\phi_i\phi_j \mid \phi_k\phi_l]_{A,B} = \int_{\Omega_A} d\vec{r}_1 \int_{\Omega_B} d\vec{r}_2 \phi_i^*(\vec{r}_1)\phi_j^*(\vec{r}_2)\frac{1}{r_{12}}\,\phi_k(\vec{r}_1)\phi_l(\vec{r}_2) \,. \tag{8}$$

The concept of effective atomic density[7] helps us to define and calculate all contributions above from the electron density. Introducing for the atom A the weight

function to the electron density function we can define the effective atomic density simply as

$$\begin{aligned} \rho^A(\vec{r}) &= w_A(\vec{r})\rho(\vec{r}) \\ \rho^A(\vec{r},\vec{r}\,') &= w_A(\vec{r})\rho(\vec{r},\vec{r}\,') \,. \end{aligned} \tag{9}$$

In the case of RHF the total energy is defined as the sum of the nuclear repulsion, E^{NN}, kinetic energy, E^{kin}, electron-nuclear attraction, E^{eN}, Coulombic electron repulsion, E^{Coul} and exchange, E^{x} , contributions, namely

$$E^{HF} = E^{NN} + E^{kin} + E^{eN} + E^{Coul} + E^{x} \,. \tag{10}$$

The nuclear repulsion is a diatomic contribution that is calculated as

$$E^{NN} = \sum_{A,B>A} E_{AB}^{NN} \,, \tag{11}$$

where the E_{AB}^{NN} for each pair of atoms is calculated as (atomic units used)

$$E_{AB}^{NN} = \frac{Z_A Z_B}{|\vec{R}_A - \vec{R}_B|} \,. \tag{12}$$

Making use of the effective atomic densities one can easily express the remaining terms. Thus, the kinetic energy is a monoatomic contribution that is calculated as

$$E^{Kin} = -\frac{1}{2}\sum_A \int \nabla^2 \rho^A(\vec{r},\vec{r}')\Big|_{\vec{r}'=\vec{r}}\, d\vec{r} \,. \tag{13}$$

The electron-nuclear attraction is a one-electron energy contribution which is divided into the sum of atomic and diatomic contribution as

$$E^{eN} = \sum_A V_A^{eN} + \sum_{A,B>A} V_{AB}^{eN} \,, \tag{14}$$

where the V_A^{eN} and V_{AB}^{eN} terms are expressed in terms of effective atomic densities as

$$\begin{aligned} V_A^{eN} &= -\int \frac{Z_A}{|\vec{r} - \vec{R}_A|}\rho^A(\vec{r})d\vec{r} \\ V_{AB}^{eN} &= -\int \frac{Z_A}{|\vec{r} - \vec{R}_A|}\rho^B(\vec{r})d\vec{r} - \int \frac{Z_B}{|\vec{r} - \vec{R}_B|}\rho^A(\vec{r})d\vec{r} \end{aligned} \,. \tag{15}$$

The Coulombic energy is a two-electron energy contribution which is also expressed as a sum of both atomic and diatomic contributions

$$E^{Coul} = \sum_A E_A^{Coul} + \sum_{A,B>A} E_{AB}^{Coul} \,, \tag{16}$$

where the E_A^{Coul} and E_{AB}^{Coul} terms are defined as

$$\begin{aligned} E_A^{Coul} &= \frac{1}{2}\int\int \frac{\rho^A(\vec{r}_1)\rho^A(\vec{r}_2)}{|\vec{r}_1-\vec{r}_2|}\, d\vec{r}_1 d\vec{r}_2 \\ E_{AB}^{Coul} &= \int\int \frac{\rho^A(\vec{r}_1)\rho^B(\vec{r}_2)}{|\vec{r}_1-\vec{r}_2|}\, d\vec{r}_1 d\vec{r}_2 \end{aligned} \,. \tag{17}$$

Finally, the exchange within Hartree-Fock is a two-electron energy contribution which involves atomic and diatomic terms as

$$E^x = \sum_A E_A^x + \sum_{A,B>A} E_{AB}^x \,, \tag{18}$$

where the E_A^x and E_{AB}^x terms are defined as

$$\begin{aligned} E_A^x &= -\frac{1}{4}\int\int \frac{\rho^A(\vec{r}_1,\vec{r}_2)\rho^A(\vec{r}_2,\vec{r}_1)}{|\vec{r}_1-\vec{r}_2|}\, d\vec{r}_1 d\vec{r}_2 \\ E_{AB}^x &= -\frac{1}{2}\int\int \frac{\rho^A(\vec{r}_1,\vec{r}_2)\rho^B(\vec{r}_2,\vec{r}_1)}{|\vec{r}_1-\vec{r}_2|}\, d\vec{r}_1 d\vec{r}_2 \end{aligned} \,. \tag{19}$$

If we take a look at the HF energy components, described on equations (11) to (19), we can divide them in two groups: the contributions obtained from one-electron integrals and the two-electron terms. Taking into account that these integrals must be performed numerically, the first group requires 3D integrations while the second group requires formally 6D integrations. Computationally, the cost of each numerical two-electron integral requires M^2 operations, where M equals the number of grid points used for the numerical integration, while the one-electron integrals require only M operations. It is clear that the bottleneck of the method is the computation of the costly numerical two-electron integrals. For each pair of atoms there is one such integral for the Coulomb term but $N_{occ}(N_{occ}+1)/2$ integrals for the exchange part, being N_{occ} the number of occupied molecular orbitals.

Another family of methods to calculate the energy from the Schrödinger equation is the Density Functional Theory (DFT). In the Kohn-Sham implementation (KS-DFT), the only difference with respect to Hartree-Fock is the exchange contribution, E^x. In the KS-

DFT energy this term is replaced by the exchange-correlation energy, E^{xc}, which is obtained as the one-electron integral

$$E^{xc} = \int \varepsilon^{xc}(\vec{r})d\vec{r} = \int \varepsilon^{xc}[\rho(\vec{r})]d\vec{r} \quad (20)$$

Here, $\varepsilon^{xc}(\vec{r})$ is the exchange-correlation energy density, which is a functional of the electron density (and its derivatives), i.e. $\varepsilon^{xc}\left[\rho,\nabla\rho,..\right]$. In KS-DFT the exchange-correlation functional is usually expressed as a sum of exchange and correlation contributions. For the exchange part, some functionals (the hybrid ones such as B3LYP) also include partially the HF exchange. Those that do not are called pure functionals.

The main problem one must face to implement similar energy decomposition for the KS-DFT energy is the exchange-correlation term, because it has a different definition for every KS-DFT functional and mainly because, contrary to HF, it is expressed as a one-electron integral. This would naturally lead to only atomic exchange-correlation contributions, destroying the chemical picture of the analysis.

The difficulty to define the one- and two-center exchange-correlation energy terms forced some groups to develop approximations of this energy contribution in two different ways. The first approximation is to do a HF-type energy decomposition with the Kohn-Sham orbitals.[8,9]The problem is that now the sum of the atomic and diatomic components does not coincide with the total energy, as implicit in equation (18). Another option is to decompose the E^{xc} into only one-center contributions,[10] losing all the information from the diatomic interactions.

1.4. KS-DFT energy partitioning

Formally, E^{xc} is a one electron quantity, for which the atomic decomposition using a 3D-space partitioning would be possible simply as

$$E^{xc} = \sum_A \int w_A(\vec{r}) \varepsilon^{xc} \left[\rho(\vec{r}) \right] d\vec{r} = \sum_A E_A^{xc} \ . \tag{21}$$

One way to calculate the atomic and diatomic exchange-correlation contribution is including the weight function twice as

$$E^{xc} = \sum_{A,B} \int w_A(\vec{r}) w_B(\vec{r}) \varepsilon^{xc} \left[\rho(\vec{r}) \right] d\vec{r} \ . \tag{22}$$

Unfortunately, the equation (22) doesn't give reasonable results about the diatomic exchange-correlation energy term. If we take a look, it can be observed that in the framework of the QTAIM theory the diatomic terms would be zero, which can hardly be put in correspondence with bonding interactions. Thus, another definition to describe the diatomic terms was still required.

In 2007, Salvador et al.[11] proposed a strategy for the 3D-space decomposition of the KS-DFT energy in which they introduce the concept of the bond order density (BODEN) to calculate the diatomic exchange-correlation energy terms.

The bond order density $\beta_{AB}(\vec{r})$ for the pair of atoms A and B is obtained by integrating the diatomic exchange density $\rho_{AB}^{x}(\vec{r},\vec{r}')$ over the coordinate $\vec{r}'$. For single determinant closed-shell wave functions, the bond order density is defined as

$$\beta_{AB}(\vec{r}) = 2 \sum_{i,j}^{nocc} \left(w_A(\vec{r}) S_{ij}^B + w_A(\vec{r}) S_{ij}^A \right) \phi_i^*(\vec{r}) \phi_j(\vec{r}) \, , \tag{23}$$

where the S_{ij}^A term corresponds to the atomic overlap matrix elements of the molecular orbitals and is defined as

$$S_{ij}^A = \int w_A(\vec{r}) \phi_i^*(\vec{r}) \phi_j(\vec{r}) d\vec{r} \ . \tag{24}$$

The BODEN represents the part of the density used to form the A-B interaction. An estimation of the diatomic exchange-correlation can be obtained by replacing the density (and its derivatives) in eq. (20) with the BODEN of the given pair of atoms. The diatomic exchange-correlation energy term then reads

$$E_{AB}^{xc} = \int \varepsilon^{xc} \left[\beta_{AB}(\vec{r}), \nabla \beta_{AB}(\vec{r}) \right] d\vec{r} \ . \tag{25}$$

For the case B=A the value of the exchange-correlation term is already provided by the equation 21, although, a correction from the diatomic contributions is required so that the sum of the atomic and diatomic contributions reproduce the total exchange-correlation energy value

$$E_A^{xc} \Leftarrow E_A^{xc} - \sum_{B \neq A} E_{AB}^{xc} / 2 \,. \tag{26}$$

It can be seen that the sum of atomic and diatomic terms gives the total E^{xc}.

The advantage of the pure KS-DFT methods is that the expensive HF-type 6D integral to calculate E^x is not required. In the case of using hybrid functionals, the calculation of E^{xc} gets computationally more complicated because every functional has a different combination of pure DFT expressions from equation (25) and HF-type contributions for the exchange.

Both the HF and KS-DFT energy decomposition schemes are implemented in the local program APOST3D.[12] The current implementation involved only the closed-shell restricted KS-DFT for a reduced number of pure and hybrid functionals, namely HFS, BLYP and B3LYP.

2. OBJECTIVES

In this project three different goals have been proposed related with the implementation of tools into the IQCC program APOST3D supervised by Dr Salvador.

The first goal is the implementation of the molecular energy decomposition for unrestricted Kohn-Sham DFT. This is the main goal of the project because its future application to open-shell systems that contains transition metals, for example the ones already studied by us,[13] can help to elucidate the differences of the metal-ligand interactions along redox processes.

The second goal is the implementation of the molecular energy decomposition to other Kohn-Sham functionals, like PBEPBE and PBE0, both for restricted and unrestricted case. With this we want to analyse to which extent the use of the BODEN for different exchange-correlation functionals, which consists in a one-electron integral, can be used to mimic the behaviour of the HF-exchange formula, which consists in a two-electron integral. For this purpose we perform a systematic study of atomic and diatomic exchange and total energy contributions for a set of molecules at the HF level and using different DFT functionals.

The last goal of this project is to improve the accuracy of the two-electron numerical integrations for reducing the integration error on the Coulombic and HF-exchange energy contributions. For this purpose we use a simple analytical model of diatomic two-electron integral.

3. METHODOLOGY

3.1. Computational details

A stablished set of 30 molecules was used to test the implementation and the posterior analysis of the decomposition of Hartree-Fock and KS-DFT energies. This set contains four main groups of molecules. The first group is formed by 5 molecules of carbon oxides and sulphur oxides, containing SO, SO_2, SO_3, CO and CO_2. The second group is formed by the series C_2H_6, C_6H_6, C_2H_4 and C_2H_2 , that perfectly represent the different bond multiplicities. A third group is formed by a set of 14 hydrides with the general formula XH_n , where X goes from Li to Cl atoms. Already in ref. 11 it was found that larger differences between the exchange energy contributions obtained with HF and pure KS-DFT could be observed due to the absence of core electrons in hydrogen. Finally, a number of other diatomic molecules were also included to the set, which again should reflect the effect of the different bond multiplicities in the value of the diatomic energy components

All calculations were carried out using Gaussian09.[14] We used different KS-DFT functionals, B3LYP and PBE, and HF with cc-pVTZ atomic basis set. Unless otherwise stated, all the geometries were optimized with the same level of theory.

All energy decompositions were carried out with the program APOST3D using the TFVC method of partition of the 3D-space. The numerical integrations were carried out using a radial grid of 70 and an angular grid of 434 points for the one-electron integrations, and a radial grid of 40 and an angular grid of 146 points for the two electron integrations.

All calculations related with the optimization of the numerical one- and two-electron integrals were realized with a self-developed Fortran77 code. For this purpose, 50 radial grid points and 110,146, 170, 266,302 and 434 angular grid points were used in our tests. The exact values of the model one-electron and two-electron integrals were calculated with the Wolfram Alpha online application.[15]

3.2. 3D numerical integrations

The numerical integrals in KS-DFT implementations typically use Becke's multicenter integration scheme.[16] It involves a combination of atomic-centered grids, each of which is defined in 3D-spherical coordinates. The numerical integration for each center involves a radial part, which is defined on the range [0, ∞), and an angular part covering the full 3D-space

In our case implementation, a Gaussian-Legendre quadrature[17] was used for the radial grid and the set of Lebedev-Laikov[18] grids was used for the angular part.

The Gaussian quadrature is an approximation to a defined integral of a one-coordinate function *f(x)* stated as a weighted sum of function values at specified integration points, within the domain of integration usually from -1 to 1. This is the case of the Gauss-Legendre quadrature. A transformation of the corresponding coordinates and its weight from [-1, 1] to $[0,\infty]$ is required, leading to

$$I=\int_0^{\infty} f(r)dr \equiv \int_{-1}^{1} f(x)dx \qquad r=r_0\frac{1+x}{1-x} \qquad dr=\frac{2r_0}{(1-x)^2}\,, \tag{27}$$

where r_0 corresponds to the distance that will contain half of the integration points. The original integral is rewritten as

$$I=\int_{-1}^{1}\frac{2r_0}{(1-x)^2} f\left(r_0\frac{1+x}{1-x}\right)dx\,, \tag{28}$$

and with the application of the Gaussian-Legendre quadrature, the integral is approximated as a weighted sum of the values of the function calculated at some pre-established integration points

$$\int_0^{\infty} f(r)dr \simeq \sum_k f(x_k)w(x_k) \qquad f(x_k)=f\left(r_0\frac{1+x}{1-x}\right) \quad w(x_k) \Leftarrow \frac{2r_0}{(1-x)^2}w(x_k)\,. \tag{29}$$

The angular grid of Lebedev consists on a given set of grid points, distributed on the surface of a sphere of radius unity, with their corresponding weights. They can be combined with a quadrature for the radial part to achieve a 3D numerical integration formally in spherical coordinates

$$\int f(\vec{r})d\vec{r} \approx \sum_k^{Nrad}\sum_i^{Nang} f(\vec{r}_{k,i})w^{rad}(r_k)w^{ang}(i)\,, \tag{30}$$

as a weighted sum of the 3D function evaluated at a set of grid points ($N_{rad} \times N_{ang}$) spherically distributed, where $\vec{r}_{k,i}=\{r_k,\phi_i\theta_i\}$.

In the case of (two-electron) 6D-integrals, a set of spherical grid points per each center must be used.

3.3. A note on sustainability

Computational chemistry uses computers to generate information such as properties of molecules or simulated experimental results. It has become a useful way to investigate materials that are too difficult to find or too expensive to purchase. It also helps chemists to get greater insight into the chemistry and make predictions before running the actual experiments, so that they can be better prepared for making observations.

From a sustainable point of view, the computational chemistry is:

i) Safer, because the experimental chemistry have an intrinsic danger associated to the experiments

ii) More clean, because there are no waste of chemical products during our tests

iii) More effective in comparison of performing experiments.

4. RESULTS AND DISCUSSION

4.1. Optimization of the rotational angles on a 6D integral

One of the main objectives of this project is the improvement of the numerical integration method used for the two-electron energy components on the APOST3D program. The numerical integrations needed to compute these contributions are very dependant of both the number and the spatial distribution of the radial and angular grid points that we use.

We have focused on the improvement of the accuracy of two-electron numerical integration over the same atom A and over two atoms along different interatomic distances. For this purpose we have used a simple analytical model for two electron integrations, representing the two-electron repulsion found in molecular systems, namely

$$I = \int\int \frac{e^{-2(x_1^2+y_1^2+z_1^2)} e^{-2(x_2^2+y_2^2+(z_2-z_0)^2)}}{\left((x_1-x_2)^2+(y_1-y_2)^2+(z_1-z_2)^2\right)^{1/2}} dx_1\, dy_1\, dz_1\, dx_2\, dy_2\, dz_2\,, \qquad (31)$$

where z_0 is used to control the type of integral. For one-center type z_0=0, and for two-center integrals z_0 determines the interatomic distance.

To approximate a two-electron integral like that of equation 31 one needs two sets of spherical grids, one for the integration over each electron coordinate, consisting of N points each. The numerical 6D integration involves the use of N^2 grid points. In the particular case of a one-center two-electron integration, N integration points can not be used because they would cancel the denominator of equation (17) and lead to a division by zero. These points are neglected but this loss affects negatively the accuracy of the integral.

Two possible solutions for an improvement of the accuracy of the numerical integration are i) increasing the number of radial and angular points or ii) to modify the spatial position of the grid for the second electron in order to use the maximum number of grid points for the integral evaluation. Computationally, the first option is highly expensive for the two-electron integrals. Then, it was thought that exploring the second option could be a good idea.

To use the maximum number of grid points, one can rotate the coordinates of the grid points for the second electron. First, the determination of which convention of coordinates defines our set of grid points is required. As we can see in the figure 2, our system can be defined on spherical coordinates or Cartesian coordinates.

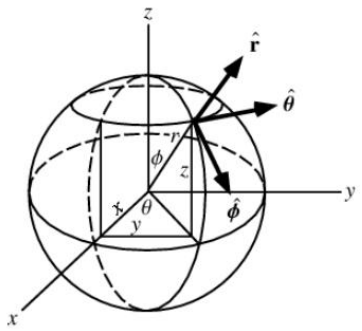

Figure 2. Representation of a sphere in Cartesian and Spherical coordinates with the corresponding angles drawn.

The Cartesian coordinate system for the integration points was used because we found in previous tests that the conversion from Cartesian to Spherical and the posterior conversion from spherical to Cartesian coordinates produce some numerical noise that would affect the accuracy of results.

The Cartesian coordinates of the angular grid can be modified (without changing the value of the associated weight) by applying rotations along one or two axis. In the case of a rotation of α and β degrees along the z and y axis, respectively, the rotated coordinates are related to the original ones as

$$\begin{aligned} x_{rot} &= \left(x_0 \cos\alpha - y_0 \sin\alpha\right)\cos\beta - z_0 \sin\beta \\ y_{rot} &= x_0 \sin\alpha + y_0 \cos\alpha \\ z_{rot} &= \left(x_0 \cos\alpha - y_0 \sin\alpha\right)\sin\beta + z_0 \cos\beta \end{aligned} \quad , \tag{32}$$

where appropriate 3D-rotation matrices have been used.

Originally, in APOST3D the second set of grid points was rotated only along the z-axis for a predefined value of $\alpha \approx 9.3$ degrees. However, we have realized that with the rotation of only this angle all points situated along the z-axis were not modified and thus still would cancel the denominator of the equation (17). Applying a rotation of β degrees along a second axis would allow the use of all grid points for the integration, depending on the particular value of α and β angles. Of course, it does not mean that the result of the numerical integration would be exact. Then, the goal is to observe how the values of α and β affect the accuracy of the numerical integration using different number of angular grid points, and whether a definite trend could be established.

The absolute integration errors of the interval [0,15] degrees along 50 steps of rotation for each combination of angles were computed using the difference between the numerical integration from our program and the exact value, which was obtained with

the Wolfram Alpha online applet. For a better presentation of the results we used two-dimensional representations of the root mean square deviation (RMSD) calculated using the integration errors from the different number of angular grid points for a determined combination of angles. We decided to mix all the different angular grids because we thought that the mixture of all of them could better represent a general case even knowing that the numerical integrations are highly dependent of the number of grid points.

The first test was the two-electron one-center integration. This case is tricky because this situation is where the maximum number of grid points cancels the denominator on equation 31. Thus, the results of the two-electron integral must have a high difference when rotating the second set of grid point. The results obtained are represented in figure 3.

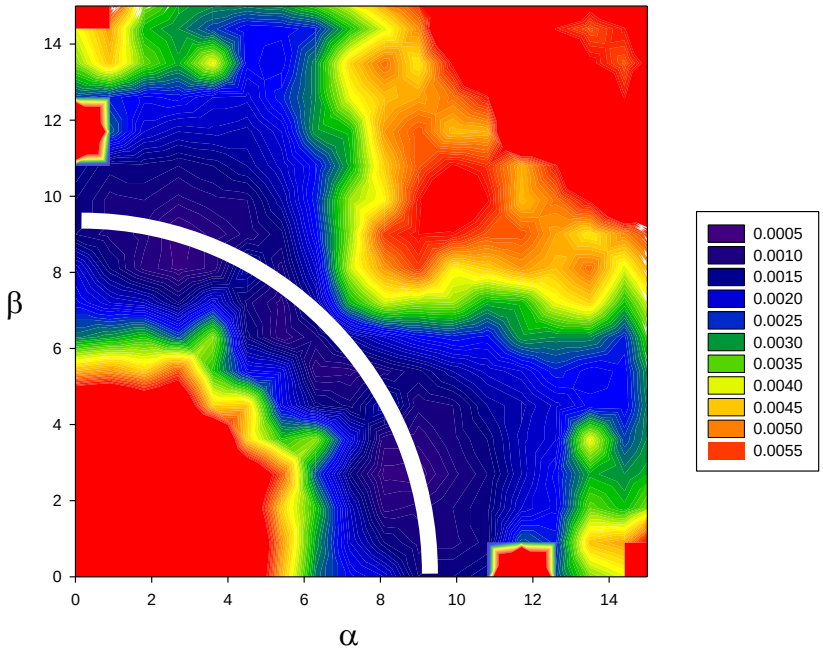

Figure 3. Two-dimension diagram of the RMSD for the two-electron one-center numerical integration error. The lowest integration error regions are indicated with a white arc.

The observed pattern is very complex. Without any rotation of the second electron grid points the integration error is very high. It corresponds with the (0,0) point in the graph. However, the rotation of the second set of grid points does not provide better results for every combination of angles. The zone in the graphic with radius smaller than 6 and higher than 12 also provides high integration errors. However, we can observe a tendency represented with a white arc with radius between 8.5 and 9.5 from the (0.0) origin in which the integration errors are minimum for our model system. There are also

some critical points, e.g. the combination of angles (12,0) or (0,12) that provide very high integration errors. We have observed that in this case there is a very high integration error for only one of the angular grids used (typically the one including 266 grid points) and this is reflected on the figure even if the other angular grids yield small errors.

The second and third tests were the 6D two-electron two-center numerical integrals with different interatomic distances. In this case, we want to see if the pattern from the first test is similar when the second electron grid points do not have the same coordinates and observe the effect of the distance in the integration error. These tests can help us to find which energy decomposition terms would contribute more to the total integration error. The results obtained for an interatomic distance of 1.5 Å and 2 Å are represented in figure 4.

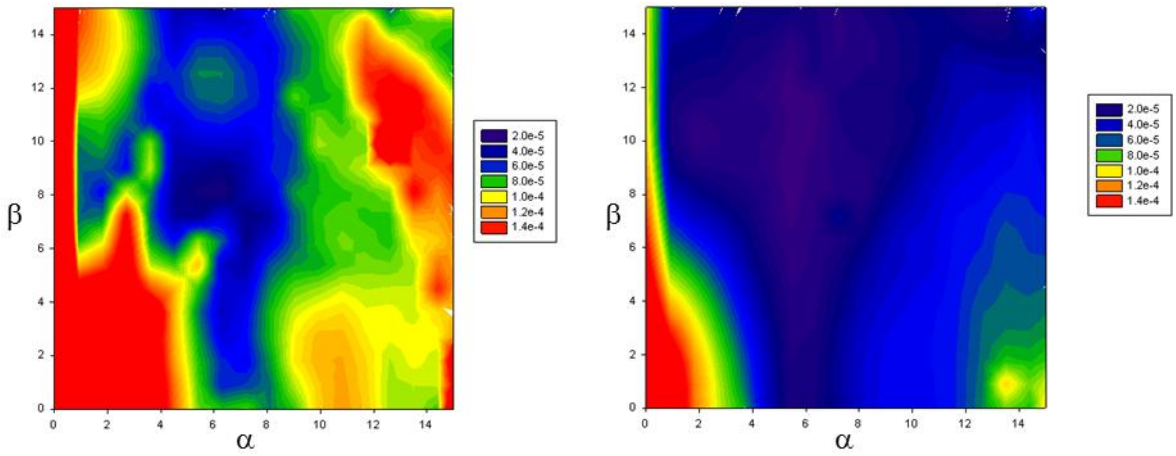

Figure 4. Two-dimension diagram of the RMSD for the two-electron two-center numerical integration for z_0=1.5 (left) and z_0 = 2 (right).

If we compare the figures 3 and 4 we can observe that the integration error is two orders of magnitude smaller in the case of two-center integrations. Moreover, the integration error also decreases significantly with the z_0 distance (figure 4 left and right). This high difference on the integration error together with the fact that it is probably unlikely to have overlapping grid points when the electrons are not in the same center allows us to affirm that the rotation of the second electron grid points is less necessary depending on the interatomic distance. From the left diagram on figure 4, we can observe that the integration error distribution is less symmetric than the one observed on figure 3. This is because our diatomic model is built along the z-axis, thus the rotation of α and β is no longer equivalent. There is a similar tendency respect the combination of angles that provides the minimum integration error, but in this case we can observe that the number of angle combinations decrease. Although, in the case of

representing the results on the same numerical scale that the figure 3, all the possible combination of angles give a reasonable small integration error.

Finally, we have implemented in APOST3D this double rotation scheme for the two-electron one-center integrations. We have performed similar analysis for a reduced set of molecules (8), and computed the error obtained in the total energy (comparing the exact number obtained with Gaussian and the sum of all one- and two-center contributions). The preliminary results are shown in figure 5.

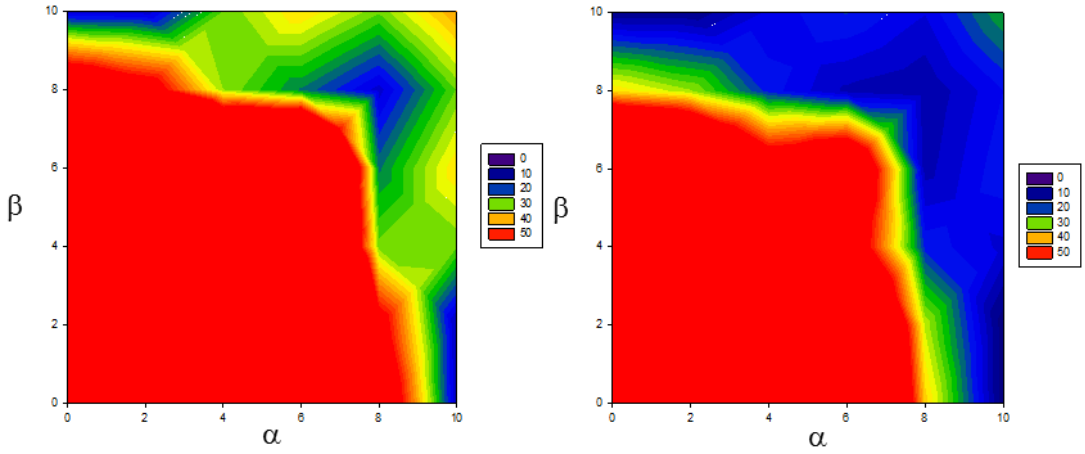

Figure 5. Two-dimension diagram of the RMSD for the total energy for a set of molecules obtained with PBEPBE functional (left) and Hartree-Fock (right). Integration errors in kcal/mol

If we compare the figure 5 with the figure 3, we can observe that the integration errors for real cases share a similar tendency with our model system. Moreover, we can affirm that the rotation of the two angles provides better results than the rotation of only one.

Two-electron two-center energy integrals are required for the Coulomb contribution both in PBEPBE and HF, but the ones associated to the exchange contribution are only present for the latter. The results indicate that for HF calculations we have a compensation of the integration error between the two implicated components, providing an integration error somewhat smaller than in the case of pure KS-DFT functionals like PBEPBE.

Both HF and PBEPBE share a the minimal integration error region for rotation angles of ca. (8,8). However, looking at the evolution of the integration error for each individual molecule of the set it appears that there is not a unique value of rotation for which the error is minimal in every case. That is, minimal error is achieved for each molecule using different rotation angles. Anyway, a wider systematic study will be required to confirm the preliminary results obtained and to extract a combination of α and β angles which minimize the integration error.

4.2. Implementation of unrestricted KS-DFT energy decomposition

The main objective of this project was the implementation of the molecular energy decomposition to unrestricted Kohn-Sham functionals to have the opportunity of working with open-shell systems in the future.

To calculate the electronic density for an open-shell system it is required to divide it into the alpha and beta contributions, taking into account the alpha and beta molecular orbitals, respectively. Then, the exchange-correlation energy is determined as the sum of the contributions for each spin, computed independently.

For the atomic and diatomic exchange energy components the same procedure must be realised as for the restricted case for the bond order density, giving in this unrestricted version the following expressions

$$\begin{aligned}
&\beta_{AB}(\vec{r}) = \beta^{\alpha}_{AB}(\vec{r}) + \beta^{\beta}_{AB}(\vec{r}) \\
&\beta^{\alpha}_{AB}(\vec{r}) = \sum_{i,j}^{N\alpha} (w_A(\vec{r}) S^{B,\alpha}_{ij} + w_B(\vec{r}) S^{A,\alpha}_{ij}) \phi^{*,\alpha}_i(\vec{r}) \phi^{\alpha}_i(\vec{r}) \,, \\
&\beta^{\beta}_{AB}(\vec{r}) = \sum_{i,j}^{N\beta} (w_A(\vec{r}) S^{B,\beta}_{ij} + w_B(\vec{r}) S^{A,\beta}_{ij}) \phi^{*,\beta}_i(\vec{r}) \phi^{\beta}_i(\vec{r})
\end{aligned} \tag{33}$$

where N_α corresponds to the number of alpha electrons, N_β corresponds to the number of beta electrons, and different atomic overlap matrix elements are used for the alpha and beta molecular orbitals. Note the absence of cross-terms, i.e. no alpha-beta mixture is necessary.

The concept of BODEN can also be applied to unrestricted open-shell systems to calculate the E_{AB}^{xc} terms by doing

$$E^{xc}_{AB} = \int \varepsilon^{xc}\left[\beta^{\alpha}_{AB}\right] d\vec{r} + \int \varepsilon^{xc}\left[\beta^{\beta}_{AB}\right] d\vec{r} \,. \tag{34}$$

In the case of gradient-corrected (GGA) functionals, the exchange-correlation is a functional of the density and its gradient. Thus, we have to compute also the gradient of the BODEN for each pair of atoms. In fact, in the unrestricted case one must compute the following three quantities

$$\begin{aligned}
\sigma^{\alpha\alpha}_{AB} &= \nabla\beta^{\alpha}_{AB} \cdot \nabla\beta^{\alpha}_{AB} \\
\sigma^{\beta\beta}_{AB} &= \nabla\beta^{\beta}_{AB} \cdot \nabla\beta^{\beta}_{AB} \,. \\
\sigma^{\alpha\beta}_{AB} &= \nabla\beta^{\alpha}_{AB} \cdot \nabla\beta^{\beta}_{AB}
\end{aligned} \tag{35}$$

If we express the KS-DFT exchange and correlation contributions separately, equation 34 is written as

$$E_{AB}^{x} = \int \varepsilon^{x}\left[\beta_{AB}^{\alpha}, \sigma_{AB}^{\alpha\alpha}\right] d\vec{r} + \int \varepsilon^{x}\left[\beta_{AB}^{\beta}, \sigma_{AB}^{\beta\beta}\right] d\vec{r}$$
$$E_{AB}^{c} = \int \varepsilon^{c}\left[\beta_{AB}^{\alpha}, \sigma_{AB}^{\alpha\alpha}, \sigma_{AB}^{\alpha\beta}\right] d\vec{r} + \int \varepsilon^{c}\left[\beta_{AB}^{\beta}, \sigma_{AB}^{\beta\beta}, \sigma_{AB}^{\alpha\beta}\right] d\vec{r} \quad , \qquad (36)$$

where it becomes evident that the exchange contribution involves only same-spin quantities. Finally, the atomic E_A^{xc} contributions are derived from the diatomic ones using equation 26, analogously to the restricted case.

We have implemented into APOST3D the expressions above for the unrestricted version of the pure functionals HFS, BLYP and PBEPBE, and hybrid B3LYP and PBE0. Both PBEPBE and PBE0 have been also implemented in the restricted version. Five new subroutines have been added to the original APOST3D version. Subroutines capable of computing the exchange-correlation density at a given set of points where obtained from the CCLRC Density Functional repository.[19]

4.3. Application to polyradical systems

After the implementation of all the corresponding definitions for the unrestricted KS-DFT functionals, we wanted to apply them to some well-known polyradical molecules. The aim of this study was twofold: i) to verify that the energy decomposition for the unrestricted Kohn-Sham functionals worked properly, and ii) apply the energy decomposition to quantify where the atomic and diatomic energy differences go to when going from low to high spin states of the polyradicals.

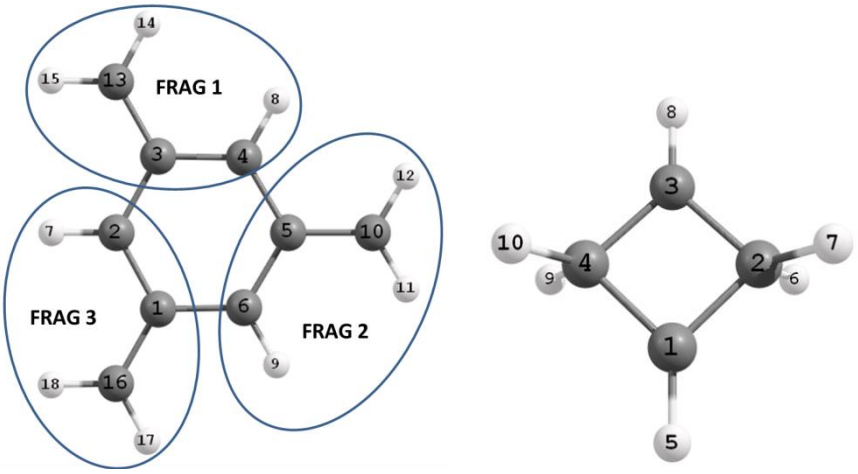

Figure 6. Polyradical molecules studied, $(CH_2CH)_2$ (right) and trimethylenebenzene (TMB) (left). Fragment definitions for the TMB molecule are indicated.

The two polyradical molecules studied are $(CH_2CH)_2$ and the trimethylenebenzene (TMB) which are represented in the figure 6. In the case of $(CH_2CH)_2$, the system

exhibits two radical centers. The electronic transition studied with the unrestricted KS-DFT energy decomposition implemented is the singlet-triplet excitation. On the other hand TMB is a triradical, exhibiting doublet and quartet electronic states.

We have performed the energy decomposition of the KS-DFT energy (B3LYP/cc-pVTZ) for all four electronic states. For illustration, in Table 1 we compile the results obtained for $(CH_2CH)_2$ in triplet state. For the atomic components we have computed the deformation energies, that is, subtracting the corresponding free-atom energy to the atomic contribution. Atomic deformation energies reflect the energy penalty the atoms pay to form the chemical bonds.

Table 1. Atomic deformation and diatomic energy components (in kcal/mol) for the triplet state of $(CH_2CH)_2$ See figure 6 for atomic numbering.

Atom	1	2	3	4	5	6	7	8	9	10
1	+150.4	-170.0	-8.5	-170.0	-161.7	-6.0	-6.0	-1.0	-6.0	-6.0
2	-170.0	+169.2	-170.0	-3.8	-3.7	-150.9	-150.9	-3.7	-1.8	-1.8
3	-8.5	-170.0	+150.4	-170.0	-1.0	-6.0	-6.0	-161.7	-6.0	-6.0
4	-170.0	-3.8	-170.0	+169.2	-3.7	-1.8	-1.8	-3.7	-150.9	-150.9
5	-161.7	-3.7	-1.0	-3.7	+22.1	+0.1	+0.1	-0.3	+0.1	+0.1
6	-6.0	-150.9	-6.0	-1.8	+0.1	+17.2	-3.6	+0.1	+0.3	+0.1
7	-6.0	-150.9	-6.0	-1.8	+0.1	-3.6	+17.2	+0.1	+0.1	+0.3
8	-1.0	-3.7	-161.7	-3.7	-0.3	+0.1	+0.1	+22.1	+0.1	+0.1
9	-6.0	-1.8	-6.0	-150.9	+0.1	+0.3	+0.1	+0.1	+17.2	-3.6
10	-6.0	-1.8	-6.0	-150.9	+0.1	+0.1	+0.3	+0.1	-3.6	+17.2

Energy components greater than +15 Kcal/mol are written in green, while those smaller than -15 Kcal/mol in red. It can be observed that the deformation energy of the atoms is very high and positive (atomic destabilization produced for the bond formation). However, there are important differences between hydrogen and carbon atoms. The electron cloud of carbon atom is bigger and much difficult to deform than that of the hydrogen. Thus, the deformation energy of a carbon must be higher which is reflected in the results.

The diatomic term for a pair of bonded atoms is highly negative (stabilization from the bond formation) because it must compensate part of the deformation energy of the atoms involved on the bond, e.g. C1 is bonded to C2, C4 and H5, with all three diatomic energies smaller than -150 kcal/mol.

The energy contributions between the distant atoms are very small in comparison with the deformation and binding energies (in absolute value). Its contribution to the total

energy is small and can be positive (reflecting small steric repulsions) or negative. For example, H6-H7 diatomic contribution is slightly negative while the H7-H8 one is positive. The former involves a geminal interaction, whereas the second a slight steric repulsion between atoms in 1,3 position.

For this system, the singlet-triplet gap is only -1.3 kcal/mol, computed at the B3LYP/cc-pVTZ level of theory. We can use the energy decomposition terms to analyse which interatomic interactions are favoured/disfavoured when going from the singlet to the ground-state triplet. We have observed small differences in both the atomic and diatomic contributions for the two electronic states, which add up to -1.4kcal/mol. That is, the integration errors, which are not negligible for each state separately (ca. 11 kcal/mol) fortunately cancel. Analyzing the results we see that going from singlet to triplet states the C2-H6 bond (and all symmetry equivalent ones) destabilize by +0.9 kcal/mol, whereas all C-C interactions, both the bonded (-0.5kcal/mol) and non-bonded (-0.7 kcal/mol) are slightly enhanced.

In this case a fortuitous error cancellation permits a quantitative analysis. This has not been the case for other similar diradical systems studied. This points out the need for improving the numerical integration method in the energy decomposition (an improved numerical integration method is required in order to describe properly the small contributions, in absolute value).

In TMB molecule the energy decomposition yields a large number of atomic and diatomic terms that make the analysis too complex. In this case one can visualize the molecule as three interacting allyl radicals, and obtain fragment energy components simply by adding all one- and two-center contributions of the atoms that form each molecular fragment. The fragments are defined as indicated in figure 6. The fragment energy decomposition results for the doublet-quartet excitation are compiled in table 2.

Table 2. Fragment analysis of the total energy differences (in Kcal/mol) between the quartet and doublet state of the TMB molecule. The overall double-quartet gap computed at the B3LYP/cc-pVTZ level of theory is -24.4 kcal/mol.

ΔE_{tot} (D-Q)	FRAG 1	FRAG 2	FRAG 3
FRAG 1	-23.3	-0.5	+25.8
FRAG 2	-0.5	-5.0	-4.4
FRAG 3	+25.8	-4.4	-20.7

The study of the energy decomposition in this molecule is not trivial because the doublet spin state of the TMB is not described properly. The broken-symmetry of the wave function complicates the interpretation of the results because the three allyl fragments are not equivalent. However, we can observe that the intra-fragment total energy difference terms are negative. It means that all allyl fragments stabilize when going from the doublet to the quartet state. The inter-fragment interaction between fragments 1-2 and 2-3 stabilizes. The most interesting results come from the fragment 3 because the 3-1 inter-fragment interaction destabilizes with a value of +25.8 kcal/mol.

These results can be better interpreted by looking at the spin densities of the fragments in the doublet state. The fragment analysis provides values of -0.19, 0.66 and 0.53 for allyl fragments 1, 2 and 3 respectively. The sum of the fragment spin densities is very close to 1, which corresponds to a doublet state, but the broken symmetry solution is far from the assumed spin down-spin up-spin up configuration of the unpaired electrons. The largest electronic redistribution after the doublet to quartet transition occurs on fragment 1, as a spin flip is required to achieve the formal quartet state. This is visualized in the analysis with a stabilization of 23.3 kcal/mol for this allyl fragment. The high stabilization of the fragment 3 is probably originated from internal spin reorganizations, whereas fragment 2 essentially remains unaffected. Thus, inter-fragment interactions involving this fragment do not vary significantly. Finally, the large stabilization of the other two allyl groups is compensated by a destabilitzation of their mutual interaction by +25.8 kcal/mol.

4.4. HF vs DFT atomic and diatomic exchange terms.

Salvador and Mayer[11] observed a very good correlation between the KS-DFT and the Hartree-Fock exchange energy not only for the diatomic but also for the atomic contributions. After including the electron correlation component using BLYP as a KS-DFT functional the correlation was still apparent.

After implementing the energy decomposition for other KS-DFT functionals for restricted and unrestricted wave functions, we wanted to observe the behaviour of the exchange KS-DFT energy in front of the HF exchange energy, calculated both with the same KS-DFT wave function. That is, we want to see to which extent the pure KS-DFT exchange atomic and diatomic terms obtained from one-electron integrations match the HF exact-exchange terms, obtained from the costly two-electron integrations.

We optimized all the geometries and calculated the wave function for the set of molecules at the B3LYP/cc-pVTZ level of theory. Then, the exchange energy

contributions for the B88, B3 and HF functionals are calculated using the previously calculated B3LYP KS orbitals.

The KS-DFT and HF atomic and diatomic exchange components are compared by linear correlation. As a result, close to perfect correlations are obtained in all cases. The results are compiled in table 3.

Table 3. Linear regressions of the atomic and diatomic exchange KS-DFT versus HF energy contributions.

	Atomic			Diatomic		
	r^2	slope	offset	r^2	slope	offset
B3 vs HF	1.0000	0.9946	-0.0290	0.9900	1.0036	0.0302
B88 vs HF	1.0000	1.0010	-0.0426	0.9845	1.0163	0.0365
PBE vs HF	1.0000	0.9961	-0.0433	0.9844	1.0075	0.0410

It was known from ref 11 that the atomic exchange energy from the hydrogen contributions affect negatively to the correlations due to the lack of core electrons. However, the authors used a different 3D-space atomic definition in their analysis that could not accommodate the large polarization of the H atoms in the molecules. In our results using the improved TFVC atomic definition, the atomic exchange energy terms are included for the hydrogens and the correlation works properly. Moreover, we can observe in table 3 that all the correlations have a slope close to 1 and a very small offset.

For this set of molecules there is a perfect correlation between the pure KS-DFT exchange energies, which require one-electron integrals to be calculated, and the hybrid KS-DFT and HF exchange energies, which require two-electron integrals. Thus, these promising results could give to us the opportunity to calculate the exchange energy contributions for hybrid KS-DFT functionals at the cost of a one-electron numerical integral.

The set of molecules studied contains only simple closed-shell molecules. The atomic and diatomic terms for four open-shell polyradical molecules are added to the B3 vs HF exchange linear correlation analysis, achieving a very good integration of them into the existing correlations.

It must be taken into account that our tests do not include organometallic molecules which are more complicated due to the quantity of electrons and the d orbitals of the

transition metals. Further studies involving this type of molecules should be included into the set to check if the tendencies observed remain.

4.5. HF vs DFT total atomic and diatomic contributions

Finally, as a last study, the atomic and diatomic total energy components were calculated for the set of molecules at different levels of theory, namely HF, PBEPBE and B3LYP methods. The optimized geometries and molecular orbitals are used for each case. The goal is to analyze to which extent the overall atomic (deformation) and diatomic terms behave for different levels of theory. The results obtained for the relevant diatomic are compiled on table 4.

All diatomic energies are negative except for the strong interatomic repulsion between the B atoms in diborane. The results are as expected for all methods. The different bond multiplicities in the hydrocarbon series are perfectly described. The diatomic energies for the single, aromatic, double and triple bond are 0.24, 0.40, 0.48 and 0.70 a.u. respectively. Linear correlations are carried out to better analyze the trends of the results for the different methods. There is also a very good correlation between the KS-DFT and HF total diatomic energies. The R^2 of all linear regressions are higher than 0.96. In figure 7 we represent the worst case, which corresponds to the PBEPBE versus HF total diatomic energy contributions.

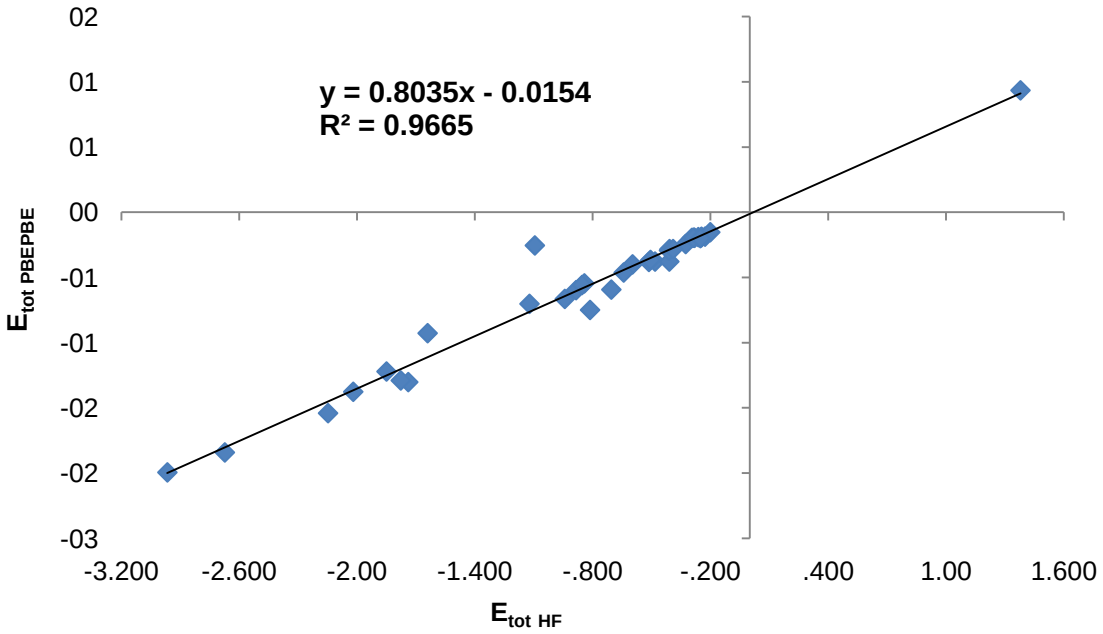

Figure 7. Representation of the PBEPBE (y-axis) in front of the HF (x-axis) total diatomic energy terms with the corresponding linear regression and its equation.

There is only one data point deviating significantly from the correlation, corresponding to the H_2S molecule. This case will be discussed later in more detail.

Table 4. Total diatomic energies (in a.u.) for the set of molecules calculated with HF, PBEPBE and B3LYP.

Bond Involved	Molecule	E_{HF}	E_{PBEPBE}	E_{B3LYP}
C-C	**C_2H_2**	-0.705	-0.711	-0.728
C-H	**C_2H_2**	-0.262	-0.228	-0.241
C-C	**C_2H_4**	-0.483	-0.453	-0.467
C-H	**C_2H_4**	-0.282	-0.234	-0.250
C-C	**C_6H_6**	-0.409	-0.338	-0.360
C-H	**C_6H_6**	-0.283	-0.234	-0.252
C-C	**C_2H_6**	-0.246	-0.229	-0.231
C-H	**C_2H_6**	-0.295	-0.235	-0.254
B-B	**B_2H_6**	1.379	1.123	1.185
B-H_b	**B_2H_6**	-0.885	-0.716	-0.757
B-H	**B_2H_6**	-0.843	-0.653	-0.698
C-O	**CO**	-1.740	-1.562	-1.608
C-O	**CO_2**	-2.020	-1.651	-1.731
S-O	**SO**	-2.148	-1.848	-1.912
S-O	**SO_2**	-2.674	-2.209	-2.328
S-O	**SO_3**	-2.967	-2.393	-2.530
H-H	**H_2**	-0.228	-0.223	-0.233
N-N	**N_2**	-0.814	-0.898	-0.900
N-O	**NO^+**	-1.851	-1.464	-1.556
C-N	**CN^-**	-1.778	-1.547	-1.609
N-O	**NO**	-1.641	-1.112	-1.197
Li-F	**LiF**	-0.327	-0.291	-0.301
F-F	**F_2**	-0.410	-0.453	-0.445
Li-H	**LiH**	-0.246	-0.224	-0.233
Be-H	**BeH_2**	-0.514	-0.456	-0.473
B-H	**BH_3**	-0.854	-0.668	-0.714
C-H	**CH_4**	-0.288	-0.233	-0.251
N-H	**NH_3**	-0.412	-0.350	-0.364
O-H	**H_2O**	-0.597	-0.478	-0.505
H-F	**HF**	-0.506	-0.438	-0.453
Na-H	**NaH**	-0.201	-0.182	-0.190
Mg-H	**MgH_2**	-0.391	-0.337	-0.353
Al-H	**AlH_3**	-0.642	-0.553	-0.575
Si-H	**SiH_4**	-0.942	-0.796	-0.835
P-H	**PH_3**	-1.122	-0.842	-0.914
S-H	**H_2S**	-1.095	-0.304	-0.344
H-Cl	**HCl**	-0.252	-0.237	-0.242

For the atomic energy terms we decided to represent the atomic deformation energies to compare more effectively the different methods. Moreover, we separated the atomic contributions involving H atoms because in this case they could also affect negatively to the correlations. The atomic deformation energies for the non-hydrogen atoms are compiled in table 5.

Table 5. Compilation of the non-hydrogen atomic deformation energy contributions (in a.u.) for the set of molecules calculated with HF, PBEPBE and B3LYP using their corresponding wave function.

Atom	Molec.	E_{HF}	E_{PBE}	E_{B3LYP}	Atom	Molec.	E_{HF}	E_{PBE}	E_{B3LYP}
C	**C_2H_2**	0.317	0.219	0.249	**N**	**CN^-**	0.921	0.618	0.662
C	**C_2H_4**	0.371	0.212	0.258	**N**	**NO**	0.939	0.572	0.639
C	**C_6H_6**	0.388	0.193	0.248	**O**	**NO**	0.626	0.275	0.321
C	**C_2H_6**	0.432	0.216	0.276	**Li**	**LiF**	0.190	0.181	0.183
B	**B_2H_6**	1.403	1.100	1.192	**F**	**LiF**	-0.006	-0.111	-0.100
C	**CO**	0.852	0.747	0.782	**F**	**F-F**	0.224	0.168	0.179
O	**CO**	0.617	0.398	0.431	**Li**	**LiH**	0.154	0.146	0.149
C	**CO_2**	2.163	1.775	1.883	**Be**	**BeH_2**	0.560	0.526	0.546
O	**CO_2**	0.556	0.316	0.351	**B**	**BH_3**	1.312	1.041	1.123
S	**SO**	1.364	1.177	1.229	**C**	**CH_4**	0.408	0.201	0.263
O	**SO**	0.795	0.326	0.276	**N**	**NH_3**	0.406	0.177	0.210
S	**SO_2**	3.207	2.723	2.882	**O**	**H_2O**	0.331	0.098	0.130
O	**SO_2**	0.740	0.468	0.510	**F**	**HF**	0.047	-0.057	-0.046
S	**SO_3**	5.273	4.401	4.666	**Na**	**NaH**	0.138	0.126	0.130
O	**SO_3**	0.674	0.395	0.437	**Mg**	**MgH_2**	0.489	0.462	0.484
N	**N_2**	0.316	0.257	0.270	**Al**	**AlH_3**	1.111	1.008	1.047
N	**NO^+**	1.437	1.135	1.217	**Si**	**SiH_4**	2.095	1.827	1.922
O	**NO^+**	0.669	0.419	0.465	**P**	**PH_3**	1.905	1.443	1.575
C	**CN^-**	0.621	0.499	0.534	**S**	**H_2S**	1.232	0.231	0.297

In this case all atomic deformation energies are positive except for the F atom in LiF. This is due to the large polarization of the atoms in this ionic molecule. That is, the atomic deformation energies also take into account charge-transfer contributions that can make the deformation energies to become negative for electronegative atoms.

Linear regressions between both KS-DFT versus HF for the non-hydrogen atomic deformation energy terms are performed obtaining in both cases R^2 higher than 0.97. Thus, we can affirm that the atomic deformation energy contributions for a HF calculation using a HF wave function correlates perfectly with the same KS-DFT contributions calculated using a KS-DFT wave function.

The atomic deformation energy contributions involving hydrogen atoms are compiled in table 6. The deformation energies are again positive in almost all cases, except when the H atom acts more clearly as a hydride (NaH and LiH).

Table 6. Compilation of the hydrogen atomic deformation energy (in a.u.) contributions for the set of molecules calculated with HF, PBEPBE and B3LYP using their corresponding wave function.

Molec.	E_{HF}	E_{PBEPBE}	E_{B3LYP}	Molec.	E_{HF}	E_{PBEPBE}	E_{B3LYP}
C_2H_2	0.072	0.041	0.044	NH_3	0.123	0.095	0.098
C_2H_4	0.066	0.026	0.030	H_2O	0.231	0.187	0.196
C_6H_6	0.065	0.023	0.027	HF	0.301	0.268	0.277
C_2H_6	0.068	0.021	0.026	NaH	0.033	-0.008	-0.010
B_2H_6	0.345	0.195	0.218	MgH_2	0.049	0.000	-0.001
B_2H_6	0.182	0.073	0.086	AlH_3	0.088	0.028	0.030
LiH	0.038	-0.008	-0.010	SiH_4	0.150	0.070	0.076
BeH_2	0.084	0.031	0.032	PH_3	0.258	0.132	0.149
BH_3	0.180	0.082	0.092	H_2S	0.318	0.052	0.058
CH_4	0.067	0.023	0.027	HCl	0.109	0.086	0.085

Again we observe a large deviation between the HF and KS-DFT values for the hydrogen atoms on H_2S. The problem with the H_2S molecule comes from the atomic partitioning of the 3D-space. In this particular case, the shape of the electron density in the interatomic H-S region is very different comparing the KS-DFT and HF results. In

HF the shape of the density is very flat, producing a quite different atomic domain for hydrogen atom. This effect can be seen already in the partial atomic charges. With KS-DFT methods the partial charge on the S atom is ca. +0.42, whereas for HF it increases up to +1.52, indicating a much larger polarization. These changes in the density are then translated into the energy decomposition analysis, providing quite different results for both methods. Excluding the H_2S molecule in the analysis, linear regressions between both KS-DFT methods vs HF for only the hydrogen deformation energies yield R^2 values higher than 0.86 in both cases,

5. CONCLUSIONS AND PERSPECTIVES

In this work we have improved the numerical integration method implemented originally in the APOST3D program by carrying a second rotation of the integration grid in the one-center two-electron integrals. It was also found that the rotation of two angles provides better results that the rotation of only one for a model system. The results obtained for actual molecules were very well simulated with our model system and we found a tendency from the combination of angles which minimizes the integration error. Wider studies are required including more complex molecules containing transition metals but the results obtained are promising.

We have implemented into APOST3D the unrestricted KS-DFT energy decomposition for the pure DFT functionals HFS, PBEPBE and BLYP and for the hybrid functionals B3LYP and PBE0. We have also implemented the restricted version of the scheme for PBEPBE and PBE0 functionals. The new capabilities of the code will allow us to study transition metal complexes in the future.

We have observed that the BODEN concept for the KS-DFT energy decomposition works perfectly for the closed- and open-shell methods implemented. A very good correlation is found comparing, for a fixed set of molecular orbitals, the KS-DFT and the HF exchange energy atomic and diatomic contributions for a relatively large set of molecules. These findings open the possibility of replacing the costly two-electron HF-type exchange integrations by the one-electron pure DFT formulation.

On the other hand, both the KS-DFT and HF energy decomposition schemes provide atomic deformation and diatomic energy components that also correlate very well with each other.

BIBLIOGRAPHY

1. Umeyama, H., Kitaura, K., Morokuma, K. (1975). *Chemical Physics Letters,* 36(1), 11-15.
2. Salvador, P., Duran, M., Mayer, I. (2001). *Journal of Chemical. Physics,* 115(3), 1153.
3. Bader, R. F. W. (1990). Atoms in Molecules: A Quantum Theory, Clarendon, Oxford.
4. Bader, R. F. W. (1991). *Chemical Reviews ,* 91(5), 893-928.
5. Mayer, I., Salvador, P. (2004). *Journal of Chemical Physics*, 120(11), 5046.
6. Mayer, I., Salvador, P. (2004). *Chemical Physics Letters,* 383(3-4), 368-375.
7. Vyboishchikov, S. F., Salvador, P., Duran, M. (2005). *Journal of Chemical Physics,* 122(24), 244110.
8. Tognetti, V., Joubert, L. (2013). *The Journal of Chemical Physics,* 138(2), 024102.
9. Tognetti, V., Joubert, L. (2014). *Physical Chemistry Chemical Physics,* 16(28), 14539.
10. Maxwell, P., Pendás, A. M., Popelier, P. L. (2016). *Physical Chemistry Chemical Physics.* (Paper ASAP).
11. Salvador, P., Mayer, I. (2007). *Journal of Chemical Physics,* 126(23), 234113.
12. Salvador P., Ramos-Cordoba, E. (2014). APOST-3D, Institute of Computational Chemistry and Catalysis, University of Girona, Girona.
13. Skara, G., Gimferrer, M., Proft, F. D., Salvador, P., Pinter, B. (2016). *Inorganic Chemistry,* 55(5), 2185-2199.
14. Frisch, M. J., et al. (2009). *Gaussian 09*, Gaussian, Inc., Wallingford CT.
15. Wolfram Alpha LLC. 2009. Wolfram|Alpha. http://www.wolframalpha.com (accessed April 15, 2016).
16. Becke, A. D., (1988). *Journal of Chemical Physics,* 88(4), 2547.
17. Stroud, A. H., Secrest, Don. (1966). *Gaussian quadrature formulas*, Prentice-Hall, Inc., Englewood Cliffs, N.J.
18. Lebedev,V. I., Laikov,D. N. (1999). *Doklady Mathematics*, 59(3), 477-481.
19. Strange, R., Manby, F. R., Knowles, P. J. (2001). *Computer Physics Communications*, 136, 310-318.